Dyssynchrony Between Endo- and Epicardial Activation in a Bilayer Model of the Left Atrium with Heterogeneous Endoepicardial Dissociation

Elham Zakeri Zafarghandi[1,2], Vincent Jacquemet[1,2]

[1] Université de Montréal, Montreal, Canada
[2] Hôpital du Sacré-Cœur de Montréal

Abstract

Endoepicardial delays in activation observed in patients with atrial fibrillation have been hypothesized to be associated with structural remodeling and layer dissociation. We aim to explore in a computer model how synchrony in endo- and epicardial activation during fibrillation is affected by local layer dissociation.

A bilayer interconnected cable model of the left atrium was used to simulate atrial fibrillation on different arrhythmogenic substrates with epicardium-only diffuse fibrosis and heterogeneous endoepicardial dissociation. Activation time series were extracted in both layers to compute endoepicardial delays and a measure of synchrony based on a coincidence window.

The simulations showed that reentrant activity was driven by the endocardium, thus generating an endoepicardial delay. Heterogeneous layer dissociation prolonged that delay locally. In regions with decoupled layers, the synchrony index was lower, illustrating how synchrony in activation may be related to the tissue structure.

1. Introduction

There is growing evidence of a three-dimensional substrate of atrial fibrillation caused by structural remodeling [1–3]. Electrical dissociation between the endo- and epicardial layers is hypothesized to induce endoepicardial dyssynchrony observed as endoepicardial delays in activation [4] and transmural breakthroughs [2, 5].

Quantification of that dyssynchrony is generally based on activation time series [4]. Accurate detection of activation in a fibrotic substrate remains challenging and delays in activation times are sensitive to electrogram fractionation, misdetection and noise, which advocates for the development of robust measures of synchrony.

In a previous study, we adapted a synchrony index [6] to quantify the synchrony between cardiac neurons [7] which have firing rates of at most a few Hz. In this paper, we investigate the application of this synchrony index to the quantification of endoepicardial asynchrony (EEA) in a computational model of endoepicardial dissociation.

2. Methods

2.1. Synchrony index

In Agmon's approach, synchronization is analyzed by pairs of time series [6]. A time series is considered the reference $t^{\mathrm{ref}} = (t_1^{\mathrm{ref}}, \ldots, t_{n_{\mathrm{ref}}}^{\mathrm{ref}})$ and the other one the target $t^{\mathrm{tar}} = (t_1^{\mathrm{tar}}, \ldots, t_{n_{\mathrm{tar}}}^{\mathrm{tar}})$. Coincidence is defined as the reference and target time series both having an event within a time interval τ. To count the number of coincidences N_c, the set W_τ combining time windows around each event of the target time series is constructed:

$$W_\tau(t^{\mathrm{tar}}) = \bigcup_{j=1}^{n_{\mathrm{tar}}} [t_j^{\mathrm{tar}} - \tau, t_j^{\mathrm{tar}} + \tau] \,, \tag{1}$$

$$N_c(t^{\mathrm{ref}}, t^{\mathrm{tar}}) = \#\{i \mid t_i^{\mathrm{ref}} \in W_\tau(t^{\mathrm{tar}})\} \,. \tag{2}$$

Some of these coincidences may have occurred by chance. These random coincidences are identified by counting those remaining after random jitter ($\pm\tau_J$) of the events of the reference time series. If the jitter of the i-th event is uniformly distributed in the interval $[t_i^{\mathrm{ref}} - \tau_J, t_i^{\mathrm{ref}} + \tau_J]$, the probability p_i of random coincidence for event i is:

$$p_i = \frac{1}{2\tau_J}\, \mu\Big([t_i^{\mathrm{ref}} - \tau_J, t_i^{\mathrm{ref}} + \tau_J] \cap W_\tau(t^{\mathrm{tar}})\Big) \,, \tag{3}$$

where $\mu(\Omega)$ is the measure (total length) of the set Ω.

The total number of random coincidences N_c^J is the sum of n_{ref} Bernoulli random variables of mean p_i. Therefore, N_c^J has mean $\langle N_c^J \rangle = \sum_{i=1}^{n_{\mathrm{ref}}} p_i$ and variance $\sigma_J^2 = \sum_{i=1}^{n_{\mathrm{ref}}} p_i(1-p_i)$. These formulas enable the analytical calculation of the probability that $N_c^J > N_c$, which provides a p-value for synchrony [6].

The bilateral jitter-based synchrony index is defined as:

$$SI_\tau^{\mathrm{bilat}}(t^{\mathrm{ref}}, t^{\mathrm{tar}}) = \beta\, \frac{N_c - \langle N_c^J \rangle}{n_{\mathrm{ref}}} \,. \tag{4}$$

The choice $\tau_J = 2\tau$ and $\beta = 2$ ensures that SI ranges between -1 (antisynchrony) and 1 (synchrony), a value of 0 meaning no synchrony [6]. The interpretation of β is that in case of perfect synchrony ($SI = 1$; $N_c = n_{\rm ref}$), a jitter of $\pm 2\tau$ will move half of the events outside the $\pm\tau$ windows around the targets, therefore $\langle N_c^J \rangle = N_c/2$.

When we want to test the hypothesis that the target time series is within a time interval τ *after* (or before if $\tau < 0$) events of the reference time series, a unilateral synchrony index can be defined by shifting the target time series by $\tau/2$ and halving the window duration:

$$SI_\tau^{\rm unilat}(t^{\rm ref}, t^{\rm tar}) = SI_{|\tau|/2}^{\rm bilat}(t^{\rm ref}, t^{\rm tar} - \tau/2)\ . \qquad (5)$$

Finally, the synchrony index can be symmetrized with respect to the two time series by setting:

$$\begin{aligned} SI_\tau(t^{\rm ref}, t^{\rm tar}) = &\frac{n_{\rm ref}}{n_{\rm tot}} SI_\tau^{\rm unilat}(t^{\rm ref}, t^{\rm tar}) \\ &+ \frac{n_{\rm tar}}{n_{\rm tot}} SI_{-\tau}^{\rm unilat}(t^{\rm tar}, t^{\rm ref})\ , \end{aligned} \qquad (6)$$

where $n_{\rm tot} = n_{\rm ref} + n_{\rm tar}$. Note the change in the sign of τ. This symmetrization is particularly appropriate when $n_{\rm ref} \approx n_{\rm tar}$. If SI_τ is close to one and $\tau > 0$, $t^{\rm tar}$ tends to occur within τ after $t^{\rm ref}$, and if $\tau < 0$, $t^{\rm tar}$ tends to occur within $|\tau|$ before $t^{\rm ref}$.

The code for computing the synchrony index is available at https://github.com/jacquemv/agmonsynchrony. It is written in python with some critical parts in Cython/C.

2.2. Atrial fibrillation modeling

A bilayer interconnected cable model of the left atrium with a resolution of 100 μm was constructed [8]. Two membrane models were used as in our previous work [9] to generate either stable rotors or meandering waves. Longitudinal and transverse conductivities were set to 4 and 1 mS/cm. Diffuse fibrosis with up to 30% density was introduced only in the epicardial layer to create endoepicardial delays in propagation [5].

Endoepicardial connections were heterogeneously distributed following random spatial patterns with a characteristic length scale from 1.6 to 11.4 mm, resulting in 75% reduction in interlayer coupling relative to control in all cases. Transmural conductivity ranged between 0.1 and 0.4 mS/cm. To enable further reduction in transmural coupling, up to four additional active intermediate nodes were inserted in the transmural connections, thus creating a total of 181,608 independent short cables connecting the two layers. This heterogeneous endoepicardial dissociation divided the atrial bilayer into connected regions (where transmural connections were located) and disconnected regions (where dyssynchronous propagation is expected to occur).

Five episodes of atrial fibrillation were initiated in each of the 288 substrates and were run for up to 6 s. Among these 1,440 episodes, 919 lasted more than 1 s (738 lasted 6 s and the others lasted 2.6 ± 1.3 s on average) and were included in subsequent analyses.

2.3. Analysis of activation delays

Activation time series were extracted at 12,669 sites in both layers to compute endoepicardial delays. The mean delay in the connected and disconnected regions was computed. The endoepicardial asynchrony (EEA) was defined as the fraction of delays > 15 ms [4].

For each simulation, all endocardial time series from sites within connected regions were concatenated, leaving at least 1 s blank space between successive time series. The same operation was performed on endocardial time series and for sites within disconnected regions, while preserving the time delays between endo- and epicardial activation. That way, SI_τ was computed on pooled time series rather than considering the statistics of multiple SI_τ with small sample size. The value of τ ranged from -10 to 30 ms.

3. Results

Figure 1 illustrates fibrillation dynamics in the presence of significant endoepicardial delays. Because of epicardial fibrosis, propagation was driven by the endocardium. Layer dissociation prolonged that delay (4.0 ± 2.2 ms within connected regions vs 11.0 ± 5.0 ms in disconnected regions) within the clinical range of endoepicardial mapping. The delay in the disconnected regions increased with the length scale of the pattern (Pearson correlation of 0.6, $p<0.001$). Note that long delays enabled the occurrence of epicardial breakthroughs.

The effect of the time window τ on the synchrony index (SI) is represented on Fig. 2. Large positive SI for $\tau > 0$ indicate that the epicardium was activated after the endocardium. The SI was significantly higher in connected vs disconnected regions (0.48 ± 0.31 vs -0.01 ± 0.16 for $\tau = 6$ ms). Synchrony index before correction for expected random coincidence (dashed curves; calculated based on all observed coincidences N_c) was higher and always positive. Overall, 98% of the p-values were < 0.01 in the connected regions and 89% in the disconnected regions, meaning that most low synchrony indices were still statistically significant.

Since disconnected regions were associated with larger delays and lower synchrony, thresholds were sought to predict (in this model) the likelihood that a time series was recorded in a disconnected region. Figure 3 shows the distribution of synchrony index ($\tau = 6$ ms) and mean endoepicardial delay. Time series in the disconnected regions had most often a delay > 6.5 ms and a $SI < 0.25$. The er-

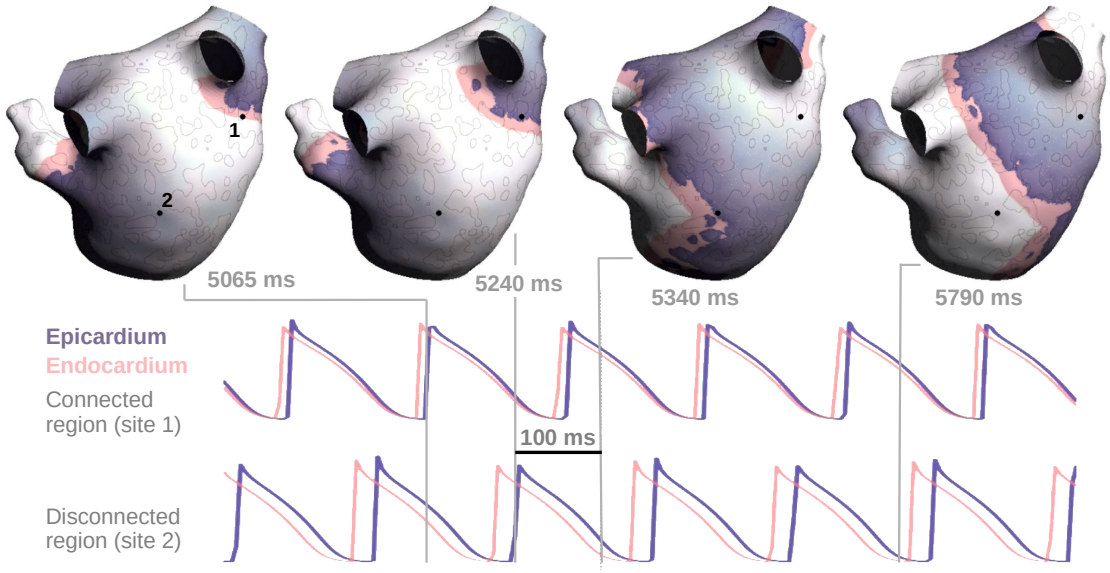

Figure 1. Examples of membrane potential maps during atrial fibrillation with endoepicardial dissociation. Epi- (blue) and endocardial (pink) maps were blended with transparency to highlight activation delays. The gray curves on the atrial surface outline the contour of the connected regions. Membrane potential traces in corresponding epi- (blue) and endocardial (pink) sites are shown below.

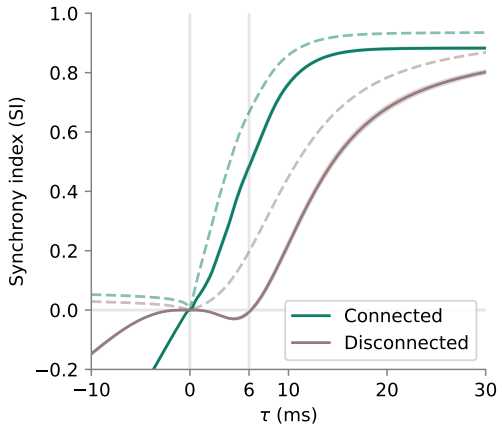

Figure 2. Synchrony index SI_τ (solid lines) as a function of τ averaged over all simulations in connected (green) and disconnected (brown) regions. Standard error on the mean (shaded areas) is barely visible because of large sample size. Dashed lines represent the synchrony index before correcting for random coincidences (N_c/n_{ref}).

ror rate for classifying connected vs disconnected regions based on the mean delay was 17% (overlap between the two distributions) and 12% when based on the synchrony index.

The synchrony index with $\tau = 15$ ms was related to 1−EEA, that is, the percentage of delays smaller than 15 ms (Fig. 4). The Pearson correlation coefficient between SI and EEA in the disconnected regions was -0.98. The distance between the data points and the diagonal SI$= 1-$EEA is explained by the correction for random coincidences that reduces SI.

4. Discussion

The synchrony index originated from the analysis of neuronal spike time series, which required robustness to noise, false detection and spontaneous activity. Applied to cardiac activation time series, this measure of synchrony has the following advantages: (1) it extends and is correlated to EEA, a measure currently used with experimental data; (2) it does not require matching pairs of endo- and epicardial activations, so it naturally handles false detection and independent propagation in the two layers; (3) it compensates for random coincidences, which become significant when τ is large; (4) it provides an easy-to-compute p-value for synchrony, which is valuable for interpreting data with lower sample size.

Its limitations for cardiac applications are that: (1) the p-value relates to the hypothesis that there is no synchrony, so p is most often very small; (2) calculation of expected random coincidences are based on events in a time window of $\pm 2\tau$ which typically contains at most one event; (3) it brings additional information over endoepicardial delays only in the case of strong endoepicardial dissociation (or large EEA).

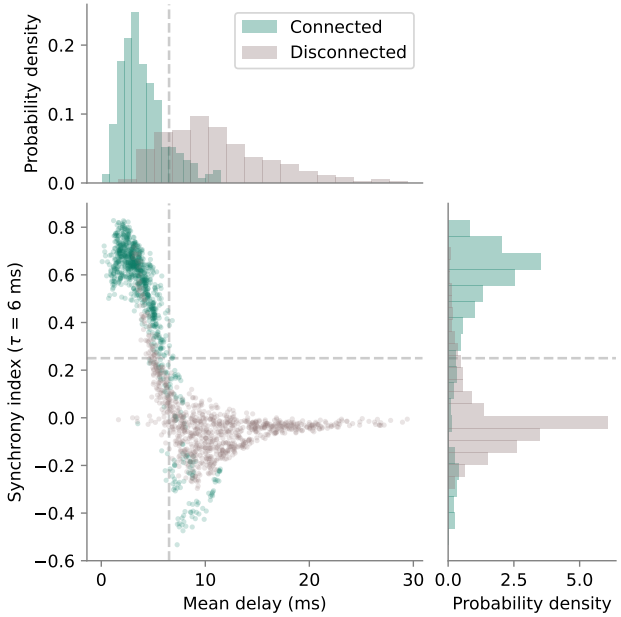

Figure 3. Synchrony index vs mean delay in connected (green) and disconnected (brown) regions for all simulations. Marginal distributions (histograms) are shown in top and right panels. The gray dashed lines (delay $= 6.5$ ms and $SI = 0.25$) are thresholds for classification between connected and disconnected regions.

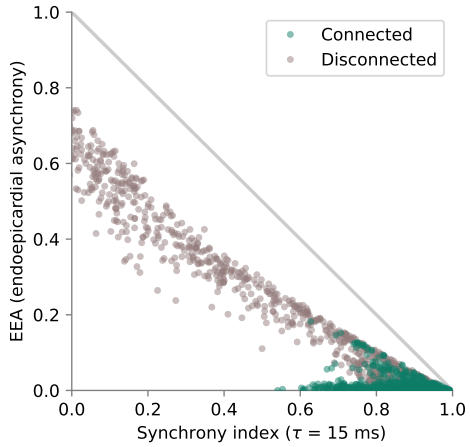

Figure 4. Synchrony indices (SI) vs endoepicardial asynchrony (EEA) for connected and disconnected regions. The diagonal line has equation SI $= 1-$ EEA.

5. Conclusions

Endoepicardial dissociation aggravates activation delays and creates dyssynchrony. The synchrony index provides a complementary experimentally applicable tool for quantitative comparison of fibrillatory activation patterns in the endo- and epicardial layers.

Acknowledgements

This work was supported by the Natural Sciences and Engineering Research Council of Canada (NSERC grant RGPIN-2020-05252).

References

[1] Ravelli F, Masè M, Cristoforetti A, et al. Quantitative assessment of transmural fibrosis profile in the human atrium: evidence for a three-dimensional arrhythmic substrate by slice-to-slice histology. Europace 2022;25(2):739–747.

[2] de Groot N, van der Does L, Yaksh A, et al. Direct proof of endo-epicardial asynchrony of the atrial wall during atrial fibrillation in humans. Circ EP 2016;9(5).

[3] Hansen BJ, Zhao J, Csepe TA, et al. Atrial fibrillation driven by micro-anatomic intramural re-entry revealed by simultaneous sub-epicardial and sub-endocardial optical mapping in explanted human hearts. Eur Heart J 2015;36(35):2390–2401.

[4] van der Does LJME, Starreveld R, Kharbanda RK, et al. Detection of endo-epicardial asynchrony in the atrial wall using one-sided unipolar and bipolar electrograms. J Cardiovasc Transl Res 2021;14(5):902–911.

[5] Gharaviri A, Bidar E, Potse M, et al. Epicardial fibrosis explains increased endo-epicardial dissociation and epicardial breakthroughs in human atrial fibrillation. Front Physiol 2020;11:68.

[6] Agmon A. A novel, jitter-based method for detecting and measuring spike synchrony and quantifying temporal firing precision. Neural Syst Circuits 2012;2(1):5.

[7] Longpré JP, Salavatian S, Beaumont E, et al. Measure of synchrony in the activity of intrinsic cardiac neurons. Physiol Meas 2014;35(4):549–66.

[8] Saliani A, Irakoze E, Jacquemet V. Simulation of diffuse and stringy fibrosis in a bilayer interconnected cable model of the left atrium. Europace 2021;23(23 Suppl 2):i169–i177.

[9] Saliani A, Biswas S, Jacquemet V. Simulation of atrial fibrillation in a non-ohmic propagation model with dynamic gap junctions. Chaos 2022;32(4):043113.

Address for correspondence:

Vincent Jacquemet
Department of pharmacology and physiology
Université de Montréal
C.P. 6128, Succursale centre-ville
Montréal (Québec) Canada H3C 3J7
vincent.jacquemet@umontreal.ca